Wideband Characterization of Holey Glide-Symmetric Parallel-Plate Waveguides

Boris Fischer and Guido Valerio
Sorbonne Université, CNRS, Laboratoire de Génie Electrique et Electronique de Paris (GeePs), 75252, Paris, France
Université Paris-Saclay, CentraleSupélec, CNRS, GeePs, 91192, Gif-sur-Yvette, France
boris.fischer@sorbonne-universite.fr

***Abstract*—Glide symmetry is a low-cost design change that enhances many properties of metallic waveguides, such as the achievable stopband, the frequency and spatial dispersion, or the effective density. But the multi-modal coupling in glide-symmetric waveguides makes it difficult to model them efficiently. This paper presents a wideband homogenization technique based on a quasi-static approximation. It yields a closed-form formula for the effective refractive index of holey glide-symmetric parallel-plate waveguides. This formula enables fast analytic studies for the properties of these waveguides, such as maximum density, isotropy, or effective constitutive parameters.**

***Index Terms*—parallel-plate waveguide, metasurface, glide symmetry, mode-matching, homogenization, effective refractive index, isotropy, characteristic impedance**

I. Introduction

Glide symmetry is a special type of higher symmetry. A waveguide is glide-symmetric when it is invariant after a translation of half-a-period in the propagation direction and a reflection with respect to the propagation plane [1].

First studied in the 60s and 70s in its one-dimensional version [2]–[4], interest for two-dimensional glide symmetry has resurfaced in recent years in the context of millimeter-wave communication. Indeed, the advantageous properties of waveguides made of metallic metasurfaces can be further enhanced when using glide symmetry [5]. Glide symmetry closes the stopband between the first and second propagating modes [6]. First, this broadens the next stopband, improving the lateral confinement for electromagnetic-bandgap waveguides and microwave devices [7]–[14]. Second, this drastically reduces the dispersion of the first mode. Ultra-wideband planar lens antennas working over tens of giga-hertz have been developed [15], [16], also exploiting the higher effective refractive index achieved by the glide-symmetric unit cells [17]. Additionally, isotropic [18] and anisotropic behaviors are improved over a larger frequency band [19], [20]. Recently, the numerical retrieval of the effective constitutive parameters [21] revealed that the magnetic response of glide-symmetric waveguides is greater than for non-glide waveguides [22], [23].

These interesting traits of glide symmetry are most notable when the gap between the metasurfaces is small, such that the multi-modal coupling between adjacent cells is non-negligible [24], [25]. This makes it difficult to model glide-symmetric waveguides. Numerical solvers result in a cumbersome process, because the simulation is slowed down by the small gap modeling, and must be performed for many different geometries to find the right design [15], [22]. It is important to remark that existing analytic models for corrugated or holey metasurfaces are unreliable in this case, due to the very strong mutual interaction of the surfaces, at the origin of the benefits of glide symmetry [24]. Therefore, new semi-analytical methods based on multi-modal transfer matrices [25] or mode-matching [26] have been designed specifically for glide-symmetric waveguides. Unfortunately, in their final steps these methods still rely on iterative solvers to obtain the features of the waveguide. In this paper, a fully-analytic model is used to study glide-symmetric waveguides.

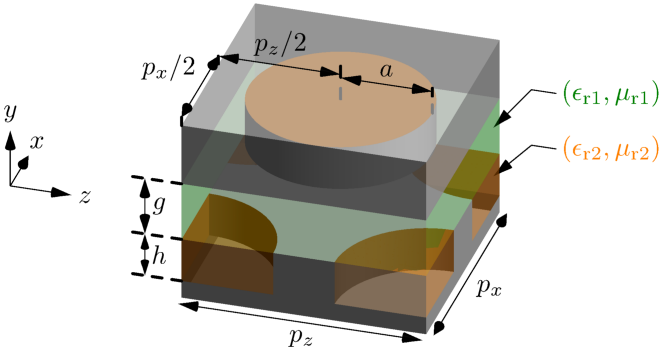

Fig. 1: Unit cell of a holey glide-symmetric parallel-plate waveguide (PPW) with circular holes, with p_z and p_x periodicities. The gap g between the metasurfaces is filled with a dielectric $(\epsilon_{r1}, \mu_{r1})$. The holes of radius a and depth h are filled with a dielectric $(\epsilon_{r2}, \mu_{r2})$.

In Section II, the dispersion equation obtained with the mode-matching method (MMM) is derived for holey glide-symmetric PPWs. A wideband homogenization technique is derived from this dispersion equation in Section III: a closed-form solution of the effective refractive index is found using a quasi-static simplification [27]. This formula is valid over a wide band, given the low dispersion induced by glide symmetry. In Section IV, it is used to validate some of the properties of these waveguides, such as the isotropy for certain hole shapes, or the higher permeability of glide-symmetric waveguides compared to their non-glide counterparts.

II. Dispersion equation of the holey PPW

A. Holey glide-symmetric PPW

A time-harmonic wave with frequency f propagates in the zx-plane of a PPW. The gap g is filled with a lossless dielectric medium 1. It is defined by its relative constitutive parameters $\epsilon_{\mathrm{r}1}$ and $\mu_{\mathrm{r}1}$, yielding $n_1 = \sqrt{\epsilon_{\mathrm{r}1}\mu_{\mathrm{r}1}}$ and $k_1 = 2\pi f n_1/c_0$. To control the propagation in the PPW, subwavelength holes of depth h are drilled periodically in the perfectly electrically conducting (PEC) plates. They are filled with a dielectric medium 2 ($\epsilon_{\mathrm{r}2}$, $\mu_{\mathrm{r}2}$).

The holes in the upper plate are shifted by $p_z/2$ in the z-direction and $p_x/2$ in the x-direction, p_z and p_x being the periods of the hole array. This shift creates glide symmetry. The unit cell of the resulting metasurface waveguide is shown in Fig. 1. Any hole cross-section can be chosen, but circular holes are a convenient manufacturing choice.

B. Modal field decomposition

Due to periodicity, the fields in the gap between the two plates are decomposed as Floquet harmonics [28, p. 607]. The field components in the propagation plane of each harmonic of orders (s,ℓ) are

$$\begin{bmatrix} E_z^{(s\ell)} \\ E_x^{(s\ell)} \end{bmatrix} = \left[\boldsymbol{a}^{(s\ell)} \sin\left(k_y^{(s\ell)} y\right) + \boldsymbol{b}^{(s\ell)} \cos\left(k_y^{(s\ell)} y\right)\right] F^{(s\ell)}, \quad (1a)$$

$$\begin{bmatrix} H_z^{(s\ell)} \\ H_x^{(s\ell)} \end{bmatrix} = \boldsymbol{Y}^{(s\ell)} \begin{bmatrix} \boldsymbol{a}^{(s\ell)} \cos\left(k_y^{(s\ell)} y\right) \\ -\boldsymbol{b}^{(s\ell)} \sin\left(k_y^{(s\ell)} y\right) \end{bmatrix} F^{(s\ell)}, \quad (1b)$$

with $F^{(s\ell)} = \mathrm{e}^{-\mathrm{j}k_z^{(s)} z - \mathrm{j}k_x^{(\ell)} x}$. The admittance matrix $\boldsymbol{Y}^{(s\ell)}$ can be found from Maxwell's equations. The Floquet wavenumbers $k_z^{(s)}$ and $k_x^{(\ell)}$ are related to the fundamental wavenumbers

$$k_z^{(s)} = k_z + s\frac{2\pi}{p_z} \quad \text{and} \quad k_x^{(\ell)} = k_x + \ell\frac{2\pi}{p_x}, \quad (2)$$

and to the vertical wavenumber ${k_y^{(s\ell)}}^2 = k_1^2 - {k_z^{(s\ell)}}^2 - {k_x^{(s\ell)}}^2$.

The fields tangential to the surface of the holes are decomposed as cylindrical waveguide modes, with field components

$$\begin{bmatrix} E_{z,m} \\ E_{x,m} \end{bmatrix} = c_m^{\mathrm{i}} \boldsymbol{e}_{\mathrm{t},m}^{\mathrm{i}}, \quad \begin{bmatrix} H_{z,m} \\ H_{x,m} \end{bmatrix} = c_m^{\mathrm{i}} Y_m^{\mathrm{i}} r_m^{\mathrm{i}} \left(\boldsymbol{e}_{\mathrm{t},m}^{\mathrm{i}} \times \boldsymbol{y}\right), \quad (3)$$

where $\mathrm{i} = \mathrm{e}, \mathrm{h}$ represents transverse magnetic (TM) or transverse electric (TE) modes, respectively. $\boldsymbol{e}_{\mathrm{t},m}^{\mathrm{i}}$ is the transverse field of each hole mode, and depends only on the hole cross-section. The wave admittances Y_m^{i} are functions of their cut-off wavenumbers k_m^{i} [29, pp. 100-1]. The coefficient $r_m^{\mathrm{i}} = -\mathrm{j}\cot(h\sqrt{k_2^2 - {k_m^{\mathrm{i}}}^2})$ is due to the total reflexion of the waveguide modes at the bottom of the holes.

C. Mode-matching method

The MMM relates the fields between different regions of the waveguide in order to obtain its dispersion equation [26]. First, the relation between adjacent half-cells is given by the generalized Floquet theorem for glide symmetry [4]. Then, the electric field continuity is enforced at the surface of the holes. From (1) and (3), the field coefficients are related such as

$$\boldsymbol{a}^{(s\ell)} = -\frac{1+(-1)^{s+\ell}}{2p_z p_x \sin\left(k_y^{(s\ell)} y\right)} \sum_m c_m^{\mathrm{i}} \left(\tilde{\boldsymbol{e}}_{\mathrm{t},m}^{\mathrm{i}(s\ell)}\right)^*, \quad (4a)$$

$$\boldsymbol{b}^{(s\ell)} = \frac{1-(-1)^{s+\ell}}{2p_z p_x \cos\left(k_y^{(s\ell)} y\right)} \sum_m c_m^{\mathrm{i}} \left(\tilde{\boldsymbol{e}}_{\mathrm{t},m}^{\mathrm{i}(s\ell)}\right)^*, \quad (4b)$$

where $\tilde{\boldsymbol{e}}_{\mathrm{t},m}^{\mathrm{i}(s\ell)}$ is the spatial Fourier transform of $\boldsymbol{e}_{\mathrm{t},m}^{\mathrm{i}}$, evaluated at $(k_z^{(s)}, k_x^{(\ell)})$. For TM modes, using Green's theorem [30, p. 431], the Fourier transform of these transverse field components can be expressed as functions of $\tilde{e}_{y,m}^{(s\ell)}$, the Fourier transform of the longitudinal field component $e_{y,m}$.

Combining (4) with the magnetic field continuity at the lower holes yields the matrix equation

$$\begin{bmatrix} \boldsymbol{M}^{\mathrm{e/e}} & \boldsymbol{M}^{\mathrm{e/h}} \\ \boldsymbol{M}^{\mathrm{e/h}^{\mathrm{H}}} & \boldsymbol{M}^{\mathrm{h/h}} \end{bmatrix} \cdot \boldsymbol{c} = 0, \quad (5)$$

where $\boldsymbol{c}$ contains the mode coefficients introduced in (3). Each matrix coefficient relates two modes. For two TM modes,

$$M_{m'm}^{\mathrm{e/e}} = \delta_{m'm} p_z p_x k_1^2 \frac{\epsilon_{\mathrm{r}2}}{\epsilon_{\mathrm{r}1}\sqrt{k_2^2 - {k_m^{\mathrm{e}}}^2}} I_m^{\mathrm{e}} \cot\left(h\sqrt{k_2^2 - {k_m^{\mathrm{e}}}^2}\right) + k_1^2 \sum_{\ell,s} f^{(s\ell)} \frac{\tilde{e}_{y,m'}^{(s\ell)} \tilde{e}_{y,m}^{(s\ell)*}}{k_{m'}^{\mathrm{e}} k_m^{\mathrm{e}}} \left[{k_z^{(s)}}^2 + {k_x^{(\ell)}}^2\right]. \quad (6)$$

For two TE modes, the coefficients have the form

$$M_{m'm}^{\mathrm{h/h}} = \delta_{m'm} p_z p_x \frac{\mu_{\mathrm{r}1}\sqrt{k_2^2 - {k_m^{\mathrm{h}}}^2}}{\mu_{\mathrm{r}2}} I_m^{\mathrm{h}} \cot\left(h\sqrt{k_2^2 - {k_m^{\mathrm{h}}}^2}\right) + \sum_{\ell,s} f^{(s\ell)} \begin{bmatrix} k_1^2 \left(\tilde{e}_{x,m'}^{\mathrm{i}'(s\ell)} \tilde{e}_{x,m}^{\mathrm{i}(s\ell)*} + \tilde{e}_{z,m'}^{\mathrm{i}'(s\ell)} \tilde{e}_{z,m}^{\mathrm{i}(s\ell)*}\right) \\ -\left(k_z^{(s)} \tilde{e}_{x,m'}^{\mathrm{i}'(s\ell)} - k_x^{(\ell)} \tilde{e}_{z,m'}^{\mathrm{i}'(s\ell)}\right) \\ \cdot \left(k_z^{(s)} \tilde{e}_{x,m}^{\mathrm{i}(s\ell)} - k_x^{(\ell)} \tilde{e}_{z,m}^{\mathrm{i}(s\ell)}\right)^* \end{bmatrix}. \quad (7)$$

Finally, for a TM and a TE mode,

$$M_{m'm}^{\mathrm{e/h}} = \mathrm{j}k_1^2 \sum_{\ell,s} f^{(s\ell)} \frac{\tilde{e}_{y,m'}^{(s\ell)}}{k_{m'}^{\mathrm{e}}} \left[k_x^{(\ell)} \tilde{e}_{x,m}^{\mathrm{h}(s\ell)} + k_z^{(s)} \tilde{e}_{z,m}^{\mathrm{h}(s\ell)}\right]^* \quad (8)$$

In (6) to (8), $\delta_{m'm}$ is the Krœnecker symbol. The squared norm of the waveguide modes is given as $I_m^{\mathrm{i}} = \iint_S \boldsymbol{e}_{\mathrm{t},m}^{\mathrm{i}} \cdot \boldsymbol{e}_{\mathrm{t},m}^{\mathrm{i}} \mathrm{d}s$. A vertical spectral function is defined as

$$f^{(s\ell)} = \begin{cases} \cot\left(\frac{g}{2} k_y^{(s\ell)}\right)/k_y^{(s\ell)} & \text{if } s+\ell \text{ is even,} \\ -\tan\left(\frac{g}{2} k_y^{(s\ell)}\right)/k_y^{(s\ell)} & \text{if } s+\ell \text{ is odd.} \end{cases} \quad (9)$$

In order for $\boldsymbol{c}$ to be a non-trivial solution of (5), the determinant of the matrix in (5) must be null. This yields the dispersion equation of the glide-symmetric waveguide.

III. Wideband homogenization

Glide symmetry has been praised for the reduced dispersion of its first propagating mode. This means that the effective refractive index of the glide-symmetric waveguide remains stable over a large band. Here, a closed-form solution of the effective refractive index n is found at low frequency.

A. Quasi-static simplification

From (2), and considering the angle θ between the propagation direction and the z-axis,

$$k_z^{(s)} \underset{k\to 0}{=} \begin{cases} s2\pi/p_z & \text{if } s \neq 0, \\ kn\cos\theta & \text{if } s = 0, \end{cases} \tag{10a}$$

$$\text{and} \quad k_x^{(\ell)} \underset{k\to 0}{=} \begin{cases} \ell 2\pi/p_x & \text{if } \ell \neq 0, \\ kn\sin\theta & \text{if } \ell = 0. \end{cases} \tag{10b}$$

As such, at low-frequency, the Fourier transforms of the field components can be evaluated at points $(s2\pi/p_z, \ell 2\pi/p_x)$. For the terms corresponding to the fundamental harmonic, the refractive index n appears according to (10). Consequently, the dispersion matrix $\boldsymbol{M}$ in (5) can be simplified, yielding

$$\boldsymbol{M} \underset{k\to 0}{=} \begin{vmatrix} k_1^2 \left(\boldsymbol{\Sigma}^{\mathrm{e}} + \frac{2n^2 \boldsymbol{u}^{\mathrm{e}} [\boldsymbol{u}^{\mathrm{e}}]^{\mathrm{H}}}{g(n_1^2 - n^2)} \right) & \mathrm{j}k_1 \frac{2nn_1 \boldsymbol{u}^{\mathrm{e}} [\boldsymbol{u}^{\mathrm{h}}]^{\mathrm{H}}}{g(n_1^2 - n^2)} \\ -\mathrm{j}k_1 \frac{2nn_1 \boldsymbol{u}^{\mathrm{h}} [\boldsymbol{u}^{\mathrm{e}}]^{\mathrm{H}}}{g(n_1^2 - n^2)} & \boldsymbol{\Sigma}^{\mathrm{h}} + \frac{2n_1^2 \boldsymbol{u}^{\mathrm{h}} [\boldsymbol{u}^{\mathrm{h}}]^{\mathrm{H}}}{g(n_1^2 - n^2)} \end{vmatrix}, \tag{11}$$

where $\boldsymbol{u}^{\mathrm{e}}$ and $\boldsymbol{u}^{\mathrm{h}}$ contain the propagation angle θ and Fourier transforms of the hole modes evaluated at $(0, 0)$. The matrices $\boldsymbol{\Sigma}^{\mathrm{e}}$ and $\boldsymbol{\Sigma}^{\mathrm{h}}$ depend on the waveguide geometry, the Fourier transforms of higher harmonics, and the propagation angle.

B. Effective refractive index

The dispersion equation of the waveguide can be further simplified at low-frequency. The determinant of the simplified matrix (11) being equal to zero, the remaining k_1-depencies can be factored out. Similarly, for the factors n and n_1, and $1/(n_1^2 - n^2)$. The resulting matrix can be written as a block-diagonal matrix containing $\boldsymbol{\Sigma}^{\mathrm{e}}$ and $\boldsymbol{\Sigma}^{\mathrm{h}}$, summed with the outer product of two vectors containing $\boldsymbol{u}^{\mathrm{e}}$ and $\boldsymbol{u}^{\mathrm{h}}$. The determinant lemma [31, p. 416] enables a scalar reformulation of this equation, yielding a second-order polynomial equation of n. The resulting closed-form solution for the refractive index is

$$n^2 = n_1^2 \frac{1 + \frac{2}{g} \left[\boldsymbol{u}^{\mathrm{h}}\right]^{\mathrm{H}} \left[\boldsymbol{\Sigma}^{\mathrm{h}}\right]^{-1} \boldsymbol{u}^{\mathrm{h}}}{1 - \frac{2}{g} \left[\boldsymbol{u}^{\mathrm{e}}\right]^{\mathrm{H}} \left[\boldsymbol{\Sigma}^{\mathrm{e}}\right]^{-1} \boldsymbol{u}^{\mathrm{e}}}, \tag{12}$$

This formula depends on the hole shape, the structure dimensions, and the propagation direction θ. As such, it can be used to design anisotropic lenses, where the θ-dependency of the refractive index is required for many different geometries. Fig. 4a illustrates such a parametric study for an anisotropic glide-symmetric PPW with rectangular holes.

Given the low dispersion of glide symmetry, (12) characterizes the waveguide over a wide frequency band. This is illustrated in Fig. 2 for different rectangular hole shapes. In this example with circular holes, depending on the desired accuracy, the formula can be used all the way up to the K-band. Other frequency bands can be targeted by scaling the structure. Moreover, the formula is much easier to implement than existing techniques due to its closed form. Finally, it is much faster than any numerical solver, because no iterative process is required, and because it enables the discrimination

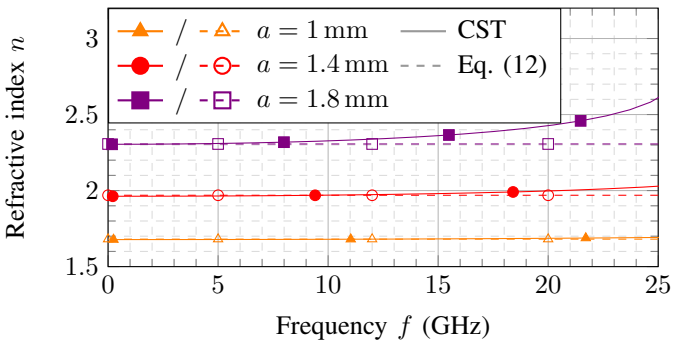

Fig. 2: Comparison between the effective refractive index n computed with (12) and the frequency-dependent index computed with CST. The considered structure is a holey glide-symmetric PPW as shown in Fig. 1, with $p_z = p_x = 4\,\mathrm{mm}$, $g = 0.1\,\mathrm{mm}$, $h = 3\,\mathrm{mm}$, and different hole radius a. In the gap, $\epsilon_{\mathrm{r1}} = 2.2$, and in the holes, $\epsilon_{\mathrm{r2}} = 4$.

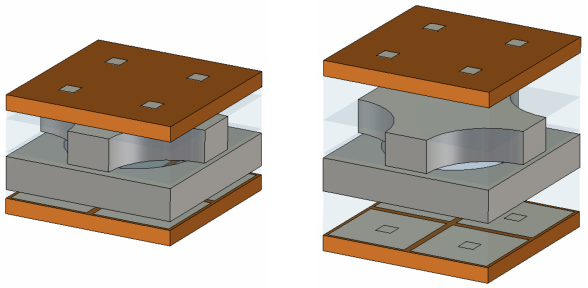

Fig. 3: Reconfigurable glide-symmetric unit cell for a compact low-loss and low-cost phase-shifter.

of modes which have no impact in (12). The execution time is divided by up to two orders of magnitude compared to CST.

We recently exploited the benefits of this formula for the preliminary studies of a reconfigurable phase-shifter, based on holey glide-symmetric metasurfaces. The reconfigurable unit cell is shown in Fig. 3. By changing the distance between an electromagnetic-bandgap layer and the holey surface with piezoelectric actuators, we vary the effective depth of the holes. The refractive index is therefore modified, yielding a continuous control of the phase shift. A larger refractive index change thus leads to a more compact phase-shifter. The closed-form formula (12) is used to rapidly discriminate different holes shapes and dielectric fillings, in order to find the candidate that yields the greatest index sensitivity with the hole depth. For example, considering equivalent hole areas, square holes yield a larger index variation than circular holes.

IV. Validation of Glide-Symmetric Properties

A. Parameter optimization

In order to design glide-symmetric microwave devices which require specific effective properties, such as planar antenna lenses, the geometry of the unit cell must be tuned. The effective refractive index formula (12) considerably accelerates

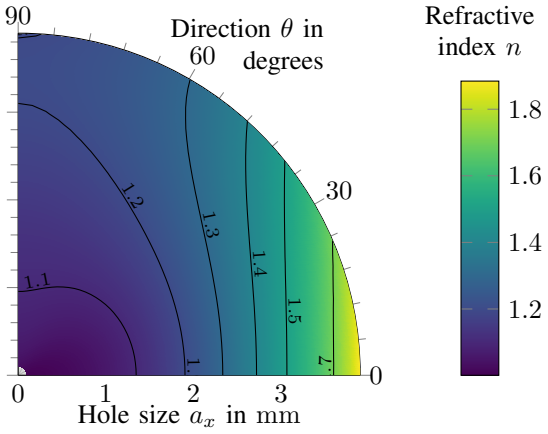

(a) $a_z = 1.5\,\mathrm{mm}$

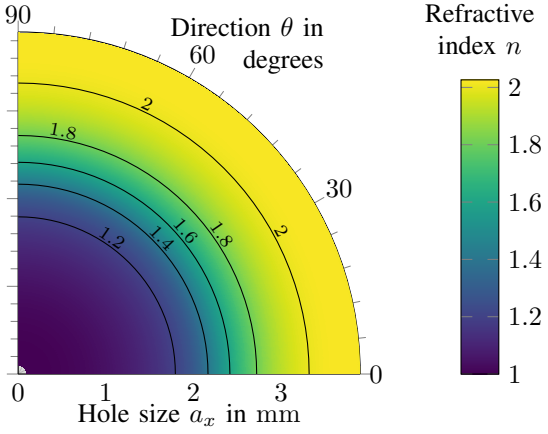

(b) $a_z = a_x$

Fig. 4: Effective refractive index of a holey glide-symmetric PPW with rectangular holes $a_z \times a_x$, as a function of the propagation angle θ. The unit cells have a size $p_z = p_x = 4\,\mathrm{mm}$, the gap is $g = 0.1\,\mathrm{mm}$, and the hole depth is $h = 5\,\mathrm{mm}$. The gap is air-filled, whereas in the holes $\epsilon_{\mathrm{r}2} = 3$ and $\mu_{\mathrm{r}2} = 1$. **(a)** Rectangular holes with fixed $a_z = 1.5\,\mathrm{mm}$ and varying a_x. **(b)** Square holes with varying $a_x = a_z$.

these parametric studies. Indeed, the effective index of a given geometry can be computed in a fraction of the time previously required by numerical solvers.

Additionally, the formula can also be used as an evaluation tool. By applying a constrained optimizer to (12), extrema values of n can be efficiently obtained. For example, in the case of a Luneburg lens, a maximum refractive index of $\sqrt{2}$ is required in the center of the lens. For a given hole shape, a maximum search on (12) would check whether or not such a value can be achieved. Further constraints could describe geometries of easier fabrication and reach an optimal shape tailored for the desired application.

B. Isotropy depending on hole cross-section

The wideband isotropy of a holey glide-symmetric PPW with triangular holes is illustrated in [18]. However, these results are obtained by solving the dispersion equation numerically, or with the commercial solver CST Microwave Studio.

The refractive index formula (12) proves that the angular dependency θ vanishes for certain hole geometries. In Fig. 4b, for square holes, the refractive index is plotted as a function of the propagation direction. The structure has $p_z = p_x = 4\,\mathrm{mm}$ and an air-filled gap $g = 0.1\,\mathrm{mm}$. The holes have varying size a, with depth $h = 5\,\mathrm{mm}$, and dielectric filling $\epsilon_{\mathrm{r}2} = 3$ and $\mu_{\mathrm{r}2} = 1$. Considering the circular form of the isoparametric curves, the structure appears to be isotropic. In fact, the closed-form index formula (12) shows analytically that n does not depend on the angle θ, proving the isotropic behavior. From (12), it comes that only TE modes in the holes are related to the spatial dispersion. Hypothetically, a structure where only TM modes propagate in the holes would always be isotropic. In the case of square holes, at low frequency, the electric field average of TE modes is polarized along either the z or the x axis. Pairs of orthogonally polarized modes can be made, whose field averages over the hole surface have the same norm. Consequently, in (12), the dispersive behavior of these modes compensates, making θ vanish.

Similar demonstrations can be made for circular holes or equilateral triangular holes. Being able to prove isotropy validates the choice of such metasurface waveguides for antenna lenses. In these lenses, the refractive index is a function of the distance from the lens center, but depending on the feed position, waves propagate through each point from different directions. Therefore, isotropy is a necessary feature for the precise design of these lenses.

C. Effective constitutive parameters

The permeability of glide-symmetric waveguides is higher than for their non-glide counterparts [22]. This enables impedance-matching scenarios between substrates with larger density disparities. Analytic knowledge about the refractive index can validate this difference, by extending the quasi-static approach back to the total field expressions.

The effective refractive index of the holey PPW is computed analytically at low frequencies with (12). Therefore, a closed form of the dispersion matrix $\boldsymbol{M}$ in (11) is known. By computing its eigenvectors in (5), the coefficients $\boldsymbol{c}$ of the hole modes are found. The coefficients of the Floquet harmonics are then given by (4) at low frequency. Consequently, for a given propagation direction in the PPW, the transverse horizontal magnetic field can be computed from (1b). The vertical electric field component is found from (1a) by applying Gauss' law.

The propagating mode is not transverse electric magnetic (TEM), and so the notion of characteristic impedance is delicate to define. However, arbitrary extensions of equivalent voltage and current can be used to characterize the input impedance of the waveguide at a chosen port. Integration of the fields between the metasurfaces gives expressions that are

representative of the effective impedance obtained numerically from S-parameters [23]. From the impedance Z and refractive index n of an effective medium, one finds $\mu = Zn$ and $\epsilon = n/Z$. These results will be compared between the glide-symmetric and non-glide cases to validate the difference of their effective behavior.

V. Conclusion

A closed-form formula of the quasi-static effective refractive index is derived for holey glide-symmetric PPWs of arbitrary hole shape. Given the low-dispersive behavior induced by glide symmetry, this formula accurately describes the effective propagation properties of the waveguide over a wide frequency range. Not only does this closed-form expression accelerate the design of glide-symmetric microwave devices such as lenses, but it also allows for a fast and wideband characterization of these structures. Through optimization of the formula, the refractive index extrema of the unit cell can be found. For hole cross-sections where analytical knowledge of the modes is at hand, isotropy can be proven. Tracing back the mode-matching process back to the field expressions, while applying the quasi-static approximation, one obtains information about the constitutive parameters of the effective propagation medium. As such, this homogenization technique opens a window into the fundamental differences between glide-symmetric and non-glide waveguides.

References

[1] O. Dahlberg, F. Ghasemifard, G. Valerio, and O. Quevedo-Teruel, "Propagation characteristics of periodic structures possessing twist and polar glide symmetries," *EPJ Applied Metamaterials*, vol. 6, p. 14, 2019.

[2] P. J. Crepeau and P. R. McIsaac, "Consequences of symmetry in periodic structures," *Proceedings of the IEEE*, vol. 52, no. 1, pp. 33–43, Jan. 1964.

[3] R. Mittra and S. Laxpati, "Propagation in a Wave Guide with Glide Reflection Symmetry," *Canadian Journal of Physics*, vol. 43, no. 2, pp. 353–372, Feb. 1965.

[4] A. Hessel, M. H. Chen, R. C. M. Li, and A. A. Oliner, "Propagation in periodically loaded waveguides with higher symmetries," *Proceedings of the IEEE*, vol. 61, no. 2, pp. 183–195, Feb. 1973.

[5] O. Quevedo-Teruel, Q. Chen, F. Mesa, N. J. G. Fonseca, and G. Valerio, "On the Benefits of Glide Symmetries for Microwave Devices," *IEEE Journal of Microwaves*, vol. 1, no. 1, pp. 457–469, Oct. 2020.

[6] R. Quesada, D. Martín-Cano, F. J. García-Vidal, and J. Bravo-Abad, "Deep-subwavelength negative-index waveguiding enabled by coupled conformal surface plasmons," *Optics Letters*, vol. 39, no. 10, pp. 2990–2993, May 2014.

[7] M. Ebrahimpouri, E. Rajo-Iglesias, Z. Sipus, and O. Quevedo-Teruel, "Low-cost metasurface using glide symmetry for integrated waveguides," in *2016 10th European Conference on Antennas and Propagation (EuCAP)*, Apr. 2016, pp. 1–2.

[8] M. Ebrahimpouri, O. Quevedo-Teruel, and E. Rajo-Iglesias, "Design of microwave components in groove gap waveguide technology implemented by holey EBG," in *2017 11th European Conference on Antennas and Propagation (EUCAP)*, Mar. 2017, pp. 746–748.

[9] E. Rajo-Iglesias, M. Ebrahimpouri, and O. Quevedo-Teruel, "Wideband Phase Shifter in Groove Gap Waveguide Technology Implemented With Glide-Symmetric Holey EBG," *IEEE Microwave and Wireless Components Letters*, vol. 28, no. 6, pp. 476–478, Jun. 2018.

[10] M. Bagheriasl, J. Sarrazin, and G. Valerio, "Reconfigurable Microwave Components Using Glide-symmetric Pin-loaded Parallel Plates," in *2020 14th European Conference on Antennas and Propagation (EuCAP)*, Mar. 2020, pp. 1–4.

[11] ——, "Reconfigurable Waveguides Using Glide-Symmetric Bed of Nails: Design of an All-Metal Switch at Millimetre-Wave Band," *arXiv:2007.08021 [eess]*, Jul. 2020.

[12] B. A. Mouris, A. Fernández-Prieto, R. Thobaben, J. Martel, F. Mesa, and O. Quevedo-Teruel, "On the Increment of the Bandwidth of Mushroom-Type EBG Structures With Glide Symmetry," *IEEE Transactions on Microwave Theory and Techniques*, vol. 68, no. 4, pp. 1365–1375, Apr. 2020.

[13] Q. Chen, F. Mesa, P. Padilla, X. Yin, and O. Quevedo-Teruel, "Efficient Leaky-Lens Antenna at 60 GHz Based on a Substrate-Integrated-Holey Metasurface," *IEEE Transactions on Antennas and Propagation*, pp. 1–1, 2020.

[14] M. Ebrahimpouri, A. Algaba Brazalez, L. Manholm, and O. Quevedo-Teruel, "Using Glide-Symmetric Holes to Reduce Leakage Between Waveguide Flanges," *IEEE Microwave and Wireless Components Letters*, vol. 28, no. 6, pp. 473–475, Jun. 2018.

[15] O. Quevedo-Teruel, M. Ebrahimpouri, and M. N. M. Kehn, "Ultrawideband Metasurface Lenses Based on Off-Shifted Opposite Layers," *IEEE Antennas and Wireless Propagation Letters*, vol. 15, pp. 484–487, Dec. 2016.

[16] O. Quevedo-Teruel, J. Miao, M. Mattsson, A. Algaba-Brazalez, M. Johansson, and L. Manholm, "Glide-Symmetric Fully Metallic Luneburg Lens for 5G Communications at Ka-Band," *IEEE Antennas and Wireless Propagation Letters*, vol. 17, no. 9, pp. 1588–1592, Sep. 2018.

[17] D. Cavallo and C. Felita, "Analytical Formulas for Artificial Dielectrics With Nonaligned Layers," *IEEE Transactions on Antennas and Propagation*, vol. 65, no. 10, pp. 5303–5311, Oct. 2017.

[18] A. Alex-Amor, G. Valerio, F. Ghasemifard, F. Mesa, P. Padilla, J. M. Fernández-González, and O. Quevedo-Teruel, "Wave Propagation in Periodic Metallic Structures with Equilateral Triangular Holes," *Applied Sciences*, vol. 10, no. 5, p. 1600, Jan. 2020.

[19] M. Ebrahimpouri and O. Quevedo-Teruel, "Ultrawideband Anisotropic Glide-Symmetric Metasurfaces," *IEEE Antennas and Wireless Propagation Letters*, vol. 18, no. 8, pp. 1547–1551, Aug. 2019.

[20] A. Alex-Amor, F. Ghasemifard, G. Valerio, M. Ebrahimpouri, P. Padilla, J. M. F. González, and O. Quevedo-Teruel, "Glide-Symmetric Metallic Structures With Elliptical Holes for Lens Compression," *IEEE Transactions on Microwave Theory and Techniques*, vol. 68, no. 10, pp. 4236–4248, Oct. 2020.

[21] X. Chen, T. M. Grzegorczyk, B.-I. Wu, J. Pacheco, and J. A. Kong, "Robust method to retrieve the constitutive effective parameters of metamaterials," *Physical Review E*, vol. 70, no. 1, p. 016608, Jul. 2004.

[22] M. Ebrahimpouri, L. F. Herran, and O. Quevedo-Teruel, "Wide-Angle Impedance Matching Using Glide-Symmetric Metasurfaces," *IEEE Microwave and Wireless Components Letters*, vol. 30, no. 1, pp. 8–11, Jan. 2020.

[23] A. C. Escobar, J. P. D. Risco, O. Quevedo-Teruel, F. Mesa, and J. D. Baena, "Retrieval of the Constitutive Parameters and Dispersion Relation of Glide-Symmetric Metamaterials via the Multimodal Transfer Matrix Method," in *2020 Fourteenth International Congress on Artificial Materials for Novel Wave Phenomena (Metamaterials)*, Sep. 2020, pp. 312–314.

[24] F. Mesa, R. Rodríguez-Berral, and F. Medina, "Considerations on the Usage of Transmission Matrices to Study the Dispersion Behavior of Glide-Symmetry Structures," in *2019 13th European Conference on Antennas and Propagation (EuCAP)*, Mar. 2019, pp. 1–4.

[25] M. Bagheriasl, O. Quevedo-Teruel, and G. Valerio, "Bloch Analysis of Artificial Lines and Surfaces Exhibiting Glide Symmetry," *IEEE Transactions on Microwave Theory and Techniques*, vol. 67, no. 7, pp. 2618–2628, Jul. 2019.

[26] F. Ghasemifard, M. Norgren, O. Quevedo-Teruel, and G. Valerio, "Analyzing Glide-Symmetric Holey Metasurfaces Using a Generalized Floquet Theorem," *IEEE Access*, vol. 6, pp. 71 743–71 750, Nov. 2018.

[27] B. Fischer and G. Valerio, "Ultra-Wideband Homogenization of a Glide-Symmetric Parallel-Plate Waveguide," in *2021 15th European Conference on Antennas and Propagation (EuCAP)*, Mar. 2021, pp. 1–4.

[28] R. E. Collin, *Field Theory of Guided Waves*, 2nd ed., ser. The IEEE/OUP Series on Electromagnetic Wave Theory. New York, NY: Inst. of Electrical and Electronics Engineers, 1991.

[29] D. M. Pozar, *Microwave Engineering*, 4th ed. Hoboken, NJ: John Wiley & Sons, Dec. 2011.

[30] J. E. Marsden and A. Tromba, *Vector Calculus*, 6th ed. New York: W.H. Freeman and Company, 2012.

[31] D. A. Harville, *Matrix Algebra from a Statistician's Perspective*. New York: Springer, 1997.